# INVESTIGATION OF CRACK PROPAGATION BY OPTICAL INTERFEROMETRIC MEASUREMENTS OF LOCAL DEFORMATION RESPONSE

**V.S. Pisarev, A.S. Dzuba, A.V. Chernov**
**Central Aero-Hydrodynamics Institute named after Prof. N.E. Zhukovsky (TsAGI)**
*VSP5335@mail.ru; dzuba@tsagi.ru; andrey.chernov@tsagi.ru*

**Keywords**: *Stress intensity factor; T-stress; Crack compliance method; Electronic speckle-pattern interferometry; Friction stir welding*

## Abstract

*New experimental technique for a determination of the stress intensity factor and the non-singular T-stress is developed, verified and implemented. The approach is based on combining the crack compliance method and optical interferometric measurements of local deformation response on small crack length increment. Initial experimental information has a form of in-plane displacement component values, which are measured by electronic speckle-pattern interferometry at some specific points located near the crack tip. The first four coefficients of Williams' formulation can be thus derived. A determination of initial experimental data in immediate neighbourhood of the notch tip is the main feature of the developed approach. In this case, it is not necessary to use complex numerical models which are connected with geometrical parameters and loading conditions of the object under study in a stage of experimental data interpretation. Moreover, an availability of high-quality interference fringe patterns, which are free from rigid-body motions, serves as a reliable indicator of real stress state in the vicinity of the notch tip. Experimental verification is performed on a base of investigation of end crack growth in trapezium contoured DCB specimen. Distributions of SIF and T-stress for cracks propagating in residual stress fields near FSW joints of two different types are constructed.*

## 1 Introduction

Friction stir welding (FSW) is a novel solid state joining process with a high potential in many modern industrial applications, especially those, which require joining aluminum alloys [1-2]. An availability of residual stresses of high level is a serious barrier that hinders a wide promotion of advanced welded structures in aerospace industry [3-6]. This means that an analysis of crack propagation process in residual stress field is the essential link inherent in optimal fatigue design of thin-walled welded structures [7].

Various experimental methods are capable of determination of stress intensity factor (SIF) and T-stress for a crack of constant length under external load increment. Unfortunately all such techniques can not be used when residual stresses are responsible for a crack growth process. That is why traditional version of the crack compliance method is currently used everywhere for describing crack behaviour under residual stress influence [3-5, 16-18]. Measurements of mechanical response caused by a small crack increment are performed by using strain gage arrays, which are located far from a crack tip. Point-wise character of the measurement procedure is not capable of reliable identifying a real type of stress state of interest. The main disadvantage of this approach resides in a necessity of creating complex numerical model, which is essential for a correct interpretation of initial experimental data. Such a model has to be created for each specific

investigated object proceeding from general loading scheme. Information on a type of stress state under study is of decisive importance for a verification of numerical model used for an interpretation of initial experimental data. All these factors negatively influence on the accuracy and reliability of final results.

This paper is devoted to a development, verification and implementation of modified version of the crack compliance method. Proposed approach is based on measuring local mechanical response caused by a small crack increment by optical interferometric methods at the nearest crack tip proximity. At first this means that there is no need for creating careful numerical model in a process of experimental data interpretation. Secondary, an availability of interference fringe patterns recorded at the crack tip proximity serves as reliable indicator of real type of stress state under study. Thus relations, who are essential for a transition from measured values to required fracture mechanics parameters, take quite simple and clear form. Moreover, developed technique is universal with respect to both a type of investigated structure and a stage of cyclic loading. This means that created approach is capable of obtaining the results of new level, which are essential for reliable describing a process of fatigue crack propagation in residual stress field. It is shown how the developed approach can be used for a determination of fracture mechanics parameters for cracks propagating in residual stress fields near FSW joints of different types.

## 2 Main Principals and Relations

The essence of modified version of the crack compliance method is a capability of recording interference fringe patterns, which correspond to a difference between two in-plane displacement component fields. Each field is referred to a crack of close but different length. The first exposure is made for a crack of initial length $a_{n-1}$ (see Fig. 1). Then initial crack length is increased by small increment $\Delta a_n$ so that new total crack length becomes equal to $a_n = a_{n-1} + \Delta a_n$ and the second exposure is performed. Required interference fringe patterns are visualized by numerical subtraction of two images recorded for two cracks [19]. Two interferograms, which are obtained by this way for thin plate with through edge crack of mode I, are shown in Fig. 2. Positive direction of $x$-axis in Fig. 1 and Fig. 2 coincides with a direction of the crack propagation.

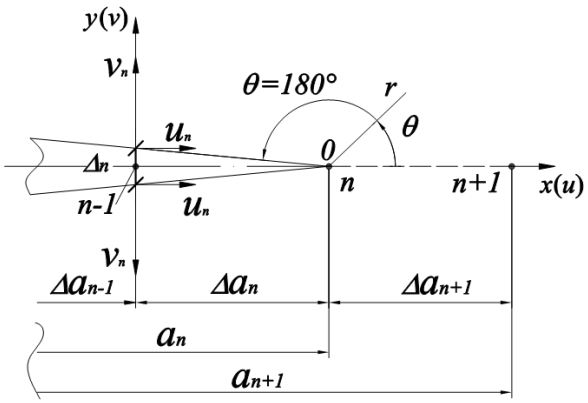


Fig.1. Polar co-ordinate system related to the crack tip and the notation adopted.

Developed procedure for deriving required fracture mechanics parameters from interference fringe patterns is based on relations between local displacement fields and fracture mechanics parameters. Required relations follow from Williams' formulation [20]. Accordingly to this approach, each in-plane displacement component at the crack tip proximity is expressed as an infinite series. When $x$-direction coincides with the crack line the expressions for mode I crack have the following form:

$$u = \sum_{n=1}^{\infty} \frac{r^{\frac{n}{2}}(1+\mu)}{E} A_n \left\{ \left[ k + \frac{n}{2} + (-1)^n \right] \cos\frac{n\theta}{2} - \frac{n}{2}\cos\frac{(n-4)\theta}{2} \right\}, \quad (1)$$

$$v = \sum_{n=1}^{\infty} \frac{r^{\frac{n}{2}}(1+\mu)}{E} A_n \left\{ \left[ k - \frac{n}{2} - (-1)^n \right] \sin\frac{n\theta}{2} + \frac{n}{2}\sin\frac{(n-4)\theta}{2} \right\},$$

where $u$ and $v$ are in-plane displacement component in direction of $x$ and $y$ axis, respectively; $E$ is the elasticity modulus of the material; $\mu$ is the Poisson's ratio; $k = (3 - \mu) / (1 + \mu)$ for plane stress and $k = (3 - 4\mu)$ for plane strain conditions; $A_n$ are constants to be determined; $r$ and $\theta$ are radial and angular distance from the crack tip as it is shown in Fig. 1.

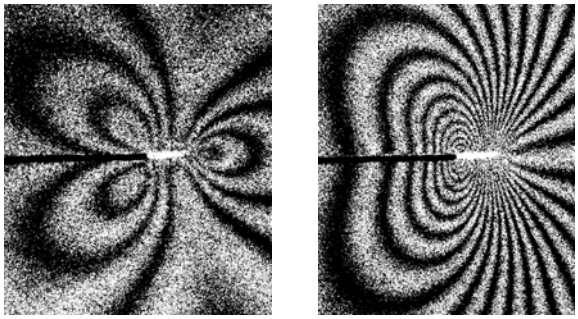

a b

Fig. 2. Specimen #MV4. Side B. Interference fringe pattern obtained in terms of in-plane displacement component $u$ (a) and $v$ (b). Initial crack length $a_{11}$ = 18.3 mm with increment $\Delta a_{12}$ = 2.0 mm.

Asymptotic formulation (1) gives the following form of elastic stress field for polar co-ordinate system with an origin at the crack tip [15]:

$$\sigma_{ij} = \frac{K_I}{\sqrt{2\pi r}} f_{ij}(\theta) + T\delta_{yi}\delta_{yj} + A_3\sqrt{2\pi r} + 0(r) \quad (2)$$

where $K_I$ is the stress intensity factor; $f_{ij}(\theta)$ is the angular function based on formulae (1); $\delta_{ij}$ is the symbol of Kronecker's determinant. The second term is called the T-stress. The value of $T$ is constant stress acting parallel to the crack plane in the direction of crack extension with a magnitude proportional to the applied gross stress. The third term $A_3$ is sometimes used as a transferability parameter like the T-stress. The non-singular term $T$ represents a tension (or compression) stress. Positive T-stress strengthens the level of crack tip stress biaxiality and leads to high crack-tip constraint while negative T-stress leads to the lost of constraint. Values of $K_I$ and T-stress are defined from relations (1) and (2) by the following way [14]:

$$K_I = A_1\sqrt{2\pi}\ ,\quad T = 4A_2 \quad (3)$$

Generally initial experimental information represents a difference in absolute values of in-plane displacement components for two cracks of length $a_n$ and $a_{n-1}$:

$$\Delta U_n = \hat{u}_n - \hat{u}_{n-1}\ ,\ \Delta V_n = v_n - v_{n-1} \quad (4)$$

Relations (4) are valid for any point belonging to the proximity of crack tip located at point $n$. But right hand sides of relations (4) include relative values of displacement components $\Delta U_n$ and $\Delta V_n$, which can not be used for direct determination of required $A_n$-values from decomposition (1). The key point of the developed approach resides in the fact that each interference fringe pattern of type shown in Fig. 2 contains a set of specific points located at the crack border immediately. Absolute values of in-plane displacement components and then coefficients $A_n$ from formulae (1) for a crack of $a_n$ length can be determined at these points.

Specific points are located along the crack line between point $n$–1 and point $n$ where displacement components $\hat{v}_{n-1}$ equal to zero before making a crack length increment. Thus interference fringe pattern shown in Fig. 2b allows us a determination of absolute values of $v$-component for each point with polar co-ordinates $0 \le r \le \Delta a_n$ and $\theta = 180^o$. A distribution of $v$ displacement component along the crack border ($\theta = 180^o$, see Fig. 1), which corresponds to the first and the third terms of infinite series (1), is expressed as:

$$v(r, \theta = \pi) = \frac{4\sqrt{r}}{E} A_1 - \frac{4r\sqrt{r}}{E} A_3 + 0(r). \quad (5)$$

Relation (5) shows that deriving $K_I$ value from (3) demands a determination of $v$-values at two points belonging to the interval $0 \le r \le \Delta a_n$, $\theta = 180^o$, as minimum. The first of them is starting point of the crack increment. A substitution of $r = \Delta a_n$ and $v(\Delta a_n, \theta{=}180^o) = v_n$ in (5) gives:

$$2v_n = \Delta_n = \frac{8\sqrt{\Delta a_n}}{E} A_1^n - \frac{8\Delta a_n\sqrt{\Delta a_n}}{E} A_3^n, \quad (6)$$

where $A^n_1$ and $A^n_3$ are coefficients of decomposition (1) for a crack of $a_n$ length. The second essential equation could be conveniently derived for the point with co-ordinate $r = \Delta a_n/2$. A substitution of $r = \Delta a_n/2$ and $v(\Delta a_n/2, \theta{=}180^o) = v^*_n$ in (5) gives:

$$2v_n^* = \Delta_n^* = \frac{8\sqrt{\Delta a_n}}{\sqrt{2}E} A_1^n - \frac{8\Delta a_n\sqrt{\Delta a_n}}{2\sqrt{2}E} A_3^n, \quad (7)$$

Coefficients $A^n_1$ and $A^n_3$ are derived from a solution of the system of linear algebraic equations (6) and (7):

$$A_1^n = \frac{E}{8\sqrt{\Delta a_n}}\left\{2\sqrt{2}\Delta_n^*(u) - \Delta_n(u)\right\},$$
$$A_3^n = -\frac{E}{4\Delta\Delta_n\sqrt{\Delta a_n}}\left\{\Delta_n(u) - \sqrt{2}\Delta_n^*(u)\right\} \quad (8)$$

A value of stress intensity factor (SIF) $K_I$ follows from a substitution of obtained result (8) into the first from relations (3):

$$K_I^n = \frac{E\sqrt{2\pi}}{8\sqrt{\Delta a_n}}\left\{2\sqrt{2}\Delta_n^* - \Delta_n\right\}. \qquad (9)$$

Taking into account only the first term from (1) leads to well-known Westergaard relation:

$$K_I^n = \frac{\Delta_n E\sqrt{2\pi}}{8\sqrt{\Delta a_n}}. \qquad (10)$$

A characterisation of T-stress values is based on a determination of $u$ displacement component directed along the crack line. A distribution of $u$ displacement component for points belonging to the crack border ($\theta = 180^o$, see Fig. 1), which corresponds to the second and the fours terms of infinite series (1), is expressed as:

$$u(r,\theta=\pi) = -\frac{4r}{E}A_2 + \frac{4r^2}{E}A_4 + 0(r). \qquad (12)$$

Relation (12) gives us the first equation essential for a determination of T-stress value. Note that all experimental parameters needed for equations (8) and (12) can be derived from interferograms pair, which correspond to $\Delta a_n$ crack length increment.

A formulation of the second required equation demands involving interference fringe pattern, which corresponds to crack length increasing from point $n$ to point $n$+1 by $\Delta a_{n+1}$ increment (see Fig. 1). Absolute value of $u$-component at specific point $n$+1 with co-ordinates $r = \Delta a_{n+1}$ and $\theta = 0$ denoted as $u_{n+1}$ depends on the first four coefficients of decomposition (1) by the following way:

$$u_{n+1} = \frac{2\sqrt{\Delta a_{n+1}}(1-\mu)}{E}A_1 + \frac{4\Delta a_{n+1}}{E}A_2^n + \\ + 2\Delta a_{n+1}\sqrt{\Delta a_{n+1}}\frac{(1-\mu)}{E}A_3^n + \frac{4(\Delta a_{n+1})^2}{E}A_4^n \qquad (13)$$

Relation (13) represents the second equation essential for a determination of T-stress because values of coefficients $A_1$ and $A_3$ are already known from relations (8). Note that a value of $u_{n+1}$ has to be derived from interference fringe pattern of type shown in Fig. 2a, which are recorded for $\Delta a_{n+1}$ crack length increment. If an estimation of T-stress value is restricted by coefficient $A^n_2$ only, the following simplified formula is valid:

$$T^n = -\frac{u_n}{\Delta a_n}E \qquad (14)$$

T-stress value (14) can be determined by using interference fringe pattern of type shown in Fig. 2a recorded for crack length increment $\Delta a_n$ only.

## 3 Measurement Procedure

Electronic speckle-pattern interferometry (ESPI) serves for a determination of in-plane displacement components [19]. Well-known optical system with normal illumination with respect to plane object surface and two symmetrical observation directions is used. Two images of the surface area of interest, which correspond to initial and final mechanical states of the object, are consequently recorded by CCD camera and stored as digital fillies. A visualization of interference fringe patterns is performed by digital subtraction of two above-mentioned images.

When a projection of illumination directions onto plane surface of the investigated object coincides with $\xi$-direction, interference fringe pattern is described as:

$$d_\xi = N\frac{\lambda}{2\sin\Psi} \qquad (15)$$

where $d_\xi$ is in-plane displacement components in $\xi$-direction; $N = \pm1; \pm2; \pm3, \ldots$ are the absolute fringe orders; $\lambda$ is the wavelength of laser illumination; $\Psi = 45^o$ is the angle between inclined illumination and normal observation directions. When $\xi$-direction coincides with $x$-axis and $y$-axis displacement component $u$ and $v$ can be derived accordingly to formula (15), respectively. Simultaneous determination of both in-plane displacement components $u$ and $v$ is reached by combining of two optical systems into united device. Diode laser with wavelength $\lambda$ = 532 nm is used as a source of the coherent illumination.

## 4 Experimental Verification

Experimental verification of the developed approach is performed by using specially designed Specimen #4MV made from aluminium alloy ($E$ = 71000 MPa, $\mu$ = 0.33) shown in Fig. 3. Working part of this specimen is a trapezium of altitude $H_T$ = 105 mm and thickness $t$ = 5 mm with dimensions of parallel sides are equal to $L_1$ = 45 mm and $L_2$ = 130 mm. A crack of length $a_0$ = 20 mm is initially made in the middle of the shortest side in a direction of the trapezium altitude. The specimen is loaded by transverse force $P$ directed orthogonally to the crack line as it is shown in Fig. 4. The main feature of trapezium contoured DCB specimen is a constancy of stress intensity factor $K_I$ for the same load value $P$ independently of a crack length. Step-by-step crack growth process is performed by narrow jewellery saw of 0.3 mm width that corresponds to notch radius $\rho$ = 0.15 mm. Such a procedure is accompanied with recording interference fringe patterns, which correspond to a difference between initial and final states of the specimen with two cracks for close load value. A scheme of the experiment involved resides in the following. External transverse load $P_{n1}$ is applied to the specimen. The first exposure is made for a crack of current length $a_{n-1}$. Then crack length is increased by small increment $\Delta a_n$ and the second exposure is made for a crack of the final length $a_n = a_{n-1} + \Delta a_n$. During a process of crack length increasing a value of acting force is slightly decreased to $P_{n2}$ due to a compliance of the force gage. Two interference fringe patterns recorded for 12$^{th}$ crack length increment on Side B are shown in Fig. 2. Ideal symmetry of presented interferograms with respect to the crack line evidently shows that stress state under considerations corresponds to mode I conditions. Perfect quality of fringe patterns ensures reliable identification of fringe orders at specific points belonging to the crack border.

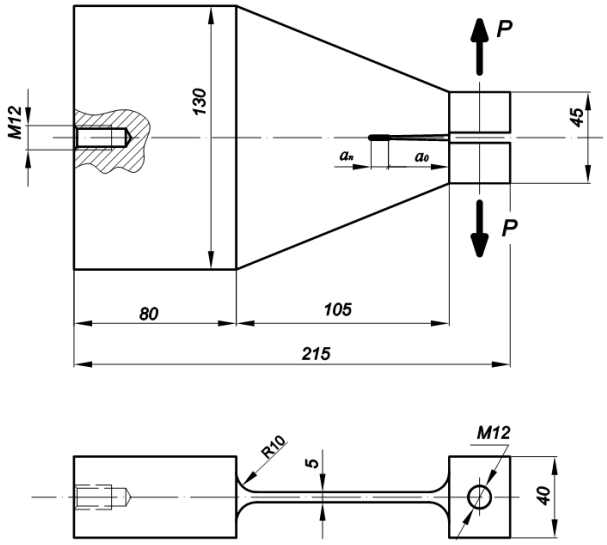


Fig. 4. Specimen #4MV and a scheme of its loading.

Interference fringe patterns are recorded for 14 crack length increments starting from initial crack length $a_0$ = 20 mm up to $a_0+a_n$ = 44.5 mm. Initial experimental information is obtained on both external faces denoted as Side A and Side B in order to increase a quality of final results. All steps involved correspond to the load range from $P_{n1}$ = 1.38 kN to $P_{n2}$ = 1.32 kg. The most reliable results related to the same loading conditions are obtained for steps 5–14. Initial experimental information obtained for these steps are listed in table 1 for Side B. Values of total crack length $a_0+a_n$ are counted from the centre of the shortest trapezium side $L_1$ = 45 mm. The values of coefficients $A^n_1$, $A^n_3$ and stress intensity factors (SIF) $K_I$ in table 1 correspond to relations (8) and (9), respectively. It should be specially note that SIF values obtained accordingly to formula (10) are less then corresponding data presented in table 1. Revealed difference reaches 25 per cent because $A^n_3$ values are not equal to zero. Data listed in table 1 show a good degree of constancy of $K_I$ values obtained for cracks of different length.

Table 1. Initial experimental information and SIF values for Specimen #MV4 obtained on Side B

| Step $n$ | $\Delta a_n$, mm | $a_0+a_n$, mm | $\Delta_n$, μm |
|---|---|---|---|
| 5 | 1.8 | 28.0 | 12.4 |
| 6 | 1.7 | 29.7 | 12.9 |
| 7 | 1.5 | 31.2 | 12.0 |
| 8 | 1.7 | 32.9 | 12.2 |
| 9 | 1.7 | 34.6 | 11.4 |
| 10 | 1.7 | 36.3 | 12.9 |
| 11 | 2.0 | 38.3 | 13.5 |
| 12 | 2.0 | 40.3 | 13.7 |
| 13 | 2.3 | 42.6 | 14.8 |
| 14 | 2.1 | 44.7 | 14.5 |
| $\Delta^*_n$, μm | $A_1^n$, kg/mm$^{3/2}$ | $A_3^n$, kg/mm$^{5/2}$ | $K_I^n$, MPa∘m$^{1/2}$ |
| 9.9 | 10.30 | 1.23 | 8.2 |
| 9.9 | 10.23 | 0.83 | 8.1 |
| 9.5 | 10.96 | 1.36 | 8.7 |
| 9.9 | 10.70 | 1.42 | 8.5 |
| 9.9 | 11.48 | 2.15 | 9.1 |
| 9.9 | 10.20 | 0.83 | 8.1 |
| 10.6 | 10.60 | 1.02 | 8.4 |
| 10.6 | 10.18 | 0.81 | 8.1 |
| 11.4 | 10.26 | 0.68 | 8.1 |
| 11.0 | 10.20 | 0.64 | 8.1 |

An estimation of the accuracy of SIF determination is performed by using a scheme of the trapezium contoured DCB specimen. In comparison with the real specimen inclined trapezium borders are conventionally lengthened up to the line of force $P$ acting (see Fig. 3). Essential relations, which connect values of force $P$ and SIF $K_I$, are presented in Murakami's handbook [21]:

$$P = \frac{K_I t\sqrt{W}}{f_I(\alpha)} \qquad (16)$$

where $t$ = 5 mm is the thickness of specimen's working part; $a_{0P}$ is total crack length conventionally counted from the line of force $P$ acting; $W$ = 120 mm is specimen's parameter; $\alpha = a_{0P}/W$. Values of $f_I(\alpha)$ function for different crack length can be derived from the formula presented in work [21]. The values of conventional total crack length $a_{0P}$ and $f_I(\alpha)$ function are listed in table 2. This table also includes SIF values obtained by averaging data corresponding to Side A and Side B for each crack length increment. Force values $P^n$ are determined by relation (16). Data from table 2 show that $P^n$ values for stages 5, 6 and 10–14 lies inside of real range of applied load from $P_{n1}$ = 1.38 kN to $P_{n2}$ = 1.32 kN. Maximal difference between real force range and $P_{n1}$ values from table 2 for stages 7–9 reaches 9 per cent. Thus we can say that developed approach represents by itself reliable tool for experimental determination of $K_I$ values.

Table 2. Averaged values of stress intensity factors and corresponding values of applied load

| Step $n$ | 5 | 6 | 7 | 8 | 9 |
|---|---|---|---|---|---|
| $a_{0P}$, mm | 42.7 | 44.4 | 46.0 | 47.6 | 49.3 |
| $f_I(\alpha)$ | 10.51 | 10.60 | 10.60 | 10.60 | 10.60 |
| $\widetilde{K}_I^n$, MPa·m$^{1/2}$ | 8.4 | 8.4 | 9.1 | 8.6 | 9.4 |
| $P^n$, kN | 1.35 | 1.34 | 1.46 | 1.39 | 1.51 |
| Step $n$ | 10 | 11 | 12 | 13 | 14 |
| $a_{0P}$, mm | 51.1 | 53.1 | 55.1 | 57.3 | 59.7 |
| $f_I(\alpha)$ | 10.60 | 10.67 | 10.68 | 10.58 | 10.56 |
| $\widetilde{K}_I^n$, MPa·m$^{1/2}$ | 8.3 | 8.4 | 8.4 | 8.4 | 8.4 |
| $P^n$, kN | 1.32 | 1.34 | 1.34 | 1.35 | 1.34 |

T-stress values obtained on Side A and Side B are very close. But initial experimental information for Side B is obtained by two optical systems simultaneously. Moreover one of these interferometers includes CCD camera pco-4000 with very high resolution (4000x2600 pixels) and wide observation field. That is why the values of coefficients $A^n_2$, $A^n_4$ and T-stresses obtained by relations (12)-(13) on Side B only are presented in table 3.

Table 3. Initial experimental information and T-stress values obtained on Side B of Specimen #MV4

| Step $n$ | $u_n$, μm | $u_{n+1}$, μm | $A_2^n$, kg/mm$^2$ | $A_4^n$, kg/mm$^3$ | $T^n$, MPa | $T^{n*}$, MPa |
|---|---|---|---|---|---|---|
| 5 | –0.76 | 1.33 | –0.30 | –0.60 | –26 | 30 |
| 6 | –0.57 | 1.52 | –0.20 | –0.44 | –17 | 23 |
| 7 | –0.38 | 1.52 | –0.41 | –0.55 | –16 | 17 |
| 8 | –0.76 | 1.14 | –0.46 | –0.72 | –18 | 31 |
| 9 | –0.57 | 1.33 | –0.60 | –0.73 | –24 | 24 |
| 10 | –0.19 | 1.33 | –0.39 | –0.34 | –15 | 8.0 |
| 11 | –0.38 | 1.52 | –0.38 | –0.37 | –15 | 13 |
| 12 | –0.38 | 1.52 | –0.29 | –0.30 | –11 | 13 |
| 13 | –0.38 | 1.71 | –0.34 | –0.28 | –13 | 11 |

An analysis of the accuracy of T-stress determination looks more difficult comparing with the procedure of $K_I$ deriving considered above. First, the number of reliable data related to experimental methods of T-stress determination is limited. Second, an availability of computer codes, which is capable of T-stress determination within appropriate accuracy, is not reliably proved by comparing analogous numerical and experimental data. One from confirmations of these facts can be found, for instance, in work [14]. Let us consider one of the problems to be solved to ensure reliable determination of T-stress values. The last column of table 3 includes T-stress values obtained by relation (14) denoted as $T^{n*}$. A difference in a sign and value of T-stresses obtained by solving a system of linear algebraic equations (12)-(13) and analogous data from relation (14) is evident. Quite similar situation takes place in work [14]. Data obtained by digital image correlation (DIC) technique for rectangular DCB specimen of 5 mm thickness show that T-stress reaches maximal value $T_2 = 16.5$ MPa for the second term of formulae (1) and then slightly decreases with increasing the term number. Thus we have some foundations to conclude that data, which correspond to terms $A^n{}_2$ and $A^n{}_4$ in developed approach, are more reliable comparing with using terms $A^n{}_2$ only.

## 5 Crack in Residual Stress Field

Developed approach is capable of determining fracture mechanics parameters for cracks in residual stress field. To confirm this fact a study of crack propagation in residual stress field near friction stir welded (FSW) joints of two different types is performed. The first object of undertaken investigation is FSW plate of dimensions 180x102x4 mm$^3$ marked as Specimen Blech 469, parent material of which is 2024 aluminium alloy. A centre of the weld of length $L = 180$ mm coincides with one from two symmetry cross-sections. Values of residual stress components, which are essential for the design of experiment based on the crack compliance method, are reliably determined by combining the hole drilling method and reflection hologram interferometry [22-23]. Revealed maximum level of tensile stress component in $x$-direction near the weld is about $\sigma_1 = 120$ MPa. The experiment by successive crack growth is performed immediately after hole drilling. Crack starting point is a hole of diameter $2r_0 = 1.5$ mm located at the point $x = 118$ mm, $y = 0$. Obtained interference fringe patterns have a form shown in Fig. 2.

It is of special interest to compare above-described data obtained for thin welded plate with analogous information that is inherent in some real structural element. That is why the second object of investigation is a specimen with FSW T-shaped joint, which simulates a wing fragment with the web. Dimensions of plane part this specimen marked as Specimen Blech 616 are 150x110x4 mm$^3$. Parent material of the specimen is AA2024-T3 aluminium alloy. Revealed maximum level of tensile stress component in $x$-direction near the weld is equal to $\sigma_1 = 120$ MPa as it takes place for Specimen Blech 469. The crack line lies in cross-section

$x$ = 97 mm. The crack starting point is a hole of diameter $2r_0$ = 2.5 mm located at the point $x$ = 97 mm, $y$ = 51 mm.

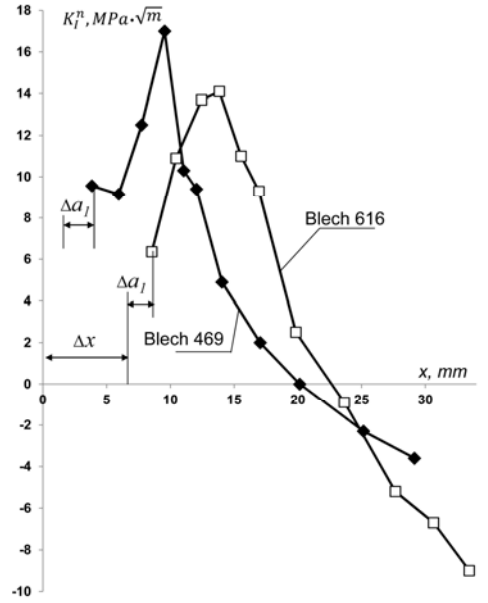


a

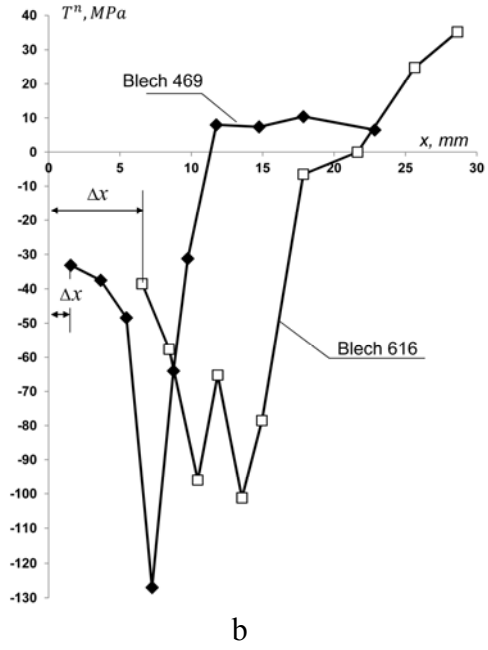


b

Fig. 4. Distributions of SIF (a) and T-stress (b) values for cracks orthogonal to friction stir welds.

Initial design of welded structural elements should be based on dependencies of SIF-values from total crack length. Dependences of T-stress from total crack length are of interest for an analysis of fatigue crack trajectory. These dependencies, which are constructed for Specimen Blech 469 and Specimen Blech 616 accordingly to relation (9) and to a solution of the system of linear algebraic equations (12)-(13), are shown in Fig. 4a and Fig. 4b for SIF and T-stress, respectively. The values of parameter $\Delta x$ represent a distances from starting point of each crack at the hole edge and central line of the weld. They are equal to $\Delta x$ = 0.8 mm and $\Delta x$ = 5.3 mm for Specimen Blech 469 and Specimen Blech 616, respectively. It should be specially noted that formula (14) gives $T$ = 0 for both specimens and any crack length increment.

## 6 Summary

New experimental method for a determination of fracture mechanics parameters by modified version of the crack compliance technique is developed verified and implemented. Its essence resides in a measurement of local deformation response on small crack length increment by electronic speckle-pattern interferometry. Obtained experimental information is capable of deriving the first four coefficients of Williams' asymptotic series and further calculations of stress intensity factor (SIF) and T-stress values. Experimental verification is performed on a base of investigation of end crack growth in trapezium contoured DCB specimen. Distributions of SIF and T-stress for cracks propagating in residual stress fields near FSW joints of two different types are constructed.

## References

[1] Mishra R.S. Friction stir processing technologies. Advanced Materials & Processing, Vol. 161, No. 10, pp 43-46, 2003.

[2] Nandan R., DebRoy T. and Bhadeshia H.K.D.H. Recent advances in friction-stir welding – Process, weldment structure and properties. Progress in Materials Science, Vol. 53, No. 6, pp 980–1023, 2008.

[3] Dalle Donna C., Lima E., Wegener J., Pyzalla A. and Buslaps T. Investigations on residual stresses in friction stir welds. *Proceedings of the 3rd International Symposium on Friction Stir Welding*, Kobe, Japan, TWI (UK), CD-ROM, 27-28 September 2001.

[4] Lima E. B. F., Wegener J., Dalle Donna C., Goerigk G., Wroblewski T., Buslaps T., Pyzalla A. and Reimers W., Dependence of the microstructure, residual stresses and texture of AA 6013 friction stir

welds on the welding process. Zeitschrift für Metallkunde, Vol. 94, pp 908-915, 2003.

[5] Milan M.T., Bose Filho W.W., Tarpani J.R., Malafaia A.M.S., Silva C.P.O., Pellizer B.C. and Pereira L.E. Residual Stress Evaluation of AA2024-T3 Friction Stir Welded Joints. Journal of Materials Engineering and Performance, Vol. 16, No. 1, pp 86-92, 2007.

[6] Martins R.V, Honkimäki V. Depth resolved strain and phase mapping of dissimilar friction stir welds using high energy synchrotron radiation. Textures and Microstructures, Vol. 35, No. 3-4, pp 145–152, 2003.

[7] James M.N., Hughes D.J., Chen Z., Lombard H., Hattingh D.G., Asquith D., Yates J.R. and Webster P.J. Residual stresses and fatigue performance. Engineering Failure Analysis, Vol. 14, No. 2, pp 384–395, 2007.

[8] Maleski M.J., Kirugulige M.S. and H.V. Tippur H.V. A Method for Measuring Mode I Crack Tip Constraint under Static and Dynamic Loading Conditions. Experimental Mechanics, Vol. 44, No. 5, pp 522-532, 2004.

[9] Hild F., Roux S. Measuring stress intensity factors with a camera: Integrated digital image correlation (I-DIC). Comptes Rendus Mécanique (C. R. Mecanique), Vol. 334, No. 1, 8-12, 2006.

[10] Yoneyama S., Morimoto Y. and Takashi M. Automatic Evaluation of Mixed-mode Stress Intensity Factors Utilizing Digital Image Correlation. Strain, Vol. 42, No 1, pp 21-29, 2006.

[11] Yoneyama S., Ogawa T., Y. and Kobayashi Y. Evaluating mixed-mode stress intensity factors from full-field displacement fields obtained by optical methods. Engineering Fracture Mechanics, Vol. 74, No. 9, pp 1399-1412, 2007.

[12] Réthoré J., Roux S. and Hild F. Noise-robust stress intensity factor determination from kinematic field measurements. Engineering Fracture Mechanics, Vol. 75, No. 13, pp 3763-3781, 2008.

[13] López-Crespo P., Burguete R.L., Patterson E.A., Shterenlikht A., Withers P.J. and Yates J.R. Study of a Crack at a Fastener Hole by Digital Image Correlation. Experimental Mechanics, Vol. 49, No. 4, pp 551–559, 2009.

[14] Yates J.R., Zanganeh M. and Tai Y.H. Quantifying crack tip displacement fields with DIC, Engineering Fracture Mechanics, Vol. 77, No. 11, pp 2063-2076, 2010.

[15] Hadj Meliani M., Azari Z., Pluvinage G. and Matvienko Yu.G. The effective T-stress estimation and crack paths emanating from U-notches Engineering Fracture Mechanics, Vol. 77, No. 11, pp 1682–1692, 2010.

[16] Prime M.B. Residual stress measurement by successive extension of a slot: The crack compliance method. Applied Mechanics Reviews, Vol. 52, No. 2, pp 75-96, 1999.

[17] Cheng W., Finie I. (2006) *Residual stress measurement and the slitting method*. USA: Springer Mechanical Engineering Series, 2006.

[18] Prime M.B. Measuring residual stress and the resulting stress intensity factor in compact tension specimen. Fatigue and Fracture of Engineering Materials and Structures, Vol. 22, No. 3, pp 195-204, 1999.

[19] Rastogi P. *Digital speckle pattern interferometry and related techniques*. Wiley, West Sussex, 2001.

[20] Williams M.L. On the stress distribution at the base of a stationary crack. ASME Journal of Applied Mechanics, Vol. 24, No. 1, pp 109–114, 1957.

[21] Murakami Y. (ed.) *Stress Intensity Factors Handbook*. Pergamon, Oxford, 1987.

[22] Pisarev V.S., Grigoriev V.D., Balalov V.V. and Chumak S.V. Residual stresses deriving from holographic interferometry data on a base of inverse problem solution. Optics & Lasers in Engineering, Vol. 42, No. 6, pp 703-726, 2004.

[23] Pisarev V.S., Bondarenko M.M., Chernov A.V. and Vinogradova A.N. General approach to residual stresses determination in thin-walled structures by combining the hole drilling method and reflection hologram interferometry. International Journal of Mechanical Sciences, Vol. 47, No. 9, pp 1350-1376, 2005.

## Copyright Statement